Available online at www.sciencedirect.com
SCIENCE DIRECT®
Surface Science 519 (2002) 125–138
SURFACE SCIENCE
www.elsevier.com/locate/susc

Infrared absorption study of physisorbed carbon monoxide on graphite

D.A. Boyd [1], F.M. Hess [2], G.B. Hess *

Department of Physics, University of Virginia, P.O. Box 400714, 382 McCormick Road, Charlottesville, VA 22904-4714, USA

Received 13 May 2002; accepted for publication 7 August 2002

Abstract

We have applied infrared reflection absorption spectroscopy (IRRAS) to the study of carbon monoxide monolayers adsorbed on a single surface of graphite (HOPG). Concurrent monitoring by laser ellipsometry determines the time of appearance of the first and second layer and of bulk CO. CO is one of the few adsorbates previously studied on graphite by IRRAS. Our spectra agree with the previously published results at 35 K and extend the temperature range to 20–40 K, including all four known solid monolayer phases in this range, and unambiguously establish which spectrum corresponds to the bilayer. Integrated absorption strength provides estimates of the average tilt of the molecular axes with respect to the surface in the nominally flat phases. Frequency shifts due to dynamic dipole coupling may contain information on the short-range correlations of tilt azimuths. We find evidence for specific tilt correlations in the commensurate phases.

PACS: 68.65.+g; 68.45.Kg; 78.30.-j
Keywords: Infrared absorption spectroscopy; Ellipsometry; Physical adsorption; Surface thermodynamics (including phase transitions); Carbon monoxide; Graphite

1. Introduction

Monolayer films of simple molecules adsorbed on graphite have been studied extensively by a variety of experimental techniques over the past 30 years as model systems of adsorption and of quasi-two-dimensional behavior [1,2]. Nevertheless gaps in knowledge remain. In particular, it is often difficult to determine molecular orientations unambiguously, even though a number of techniques give relevant information. Complete structural information can be obtained in principle by modeling neutron or low energy electron diffraction intensities. In practice the inference of orientations often relies heavily on symmetry and steric considerations. For suitable molecules, infrared reflection absorption spectroscopy (IRRAS) can give rather direct information on the orientation of molecular vibration axes with respect to the

* Corresponding author. Tel.: +1-434-924-3781; fax: +1-434-924-4576.
E-mail address: gbh@virginia.edu (G.B. Hess).
[1] Present address: The Thomas J. Watson Sr., Laboratories of Applied Physics, The California Institute of Technology, MS 128-95 Pasadena, CA 91125, USA.
[2] Present address: Department of Physics, University of Illinois, Urbana-Champaign, IL 61801, USA.

0039-6028/02/$ - see front matter
PII: S0039-6028(02)02207-0

surface normal [3] and possibly also indirect information on other orientation parameters.

Highly oriented pyrolytic graphite (HOPG) is a favorable adsorption substrate for techniques that require only a small surface area (of order 1 cm^2 or less). A clean surface that is atomically flat over patches of diameter 100–1000 nm can be prepared simply by cleaving in air and heating in vacuum. On a visible scale the surface is slightly wavy. Although the reflectivity is not as high as for metals, it is sufficiently good in the mid-infrared that the usual surface selection rule is obeyed: There is significant coupling only to the projection of a dynamic dipole moment perpendicular to the surface.

IRRAS has been applied extensively to chemisorption on metals [4–6]. Infrared absorption in transmission has been applied to physisorption on cleaved crystal surfaces; in particular, Heidberg et al. [7] and Ewing [8] have examined monolayers of adsorbates including CO, CO_2 and CH_4 on NaCl and on MgO. Only limited work has been done on a single-surface graphite substrate: Heidberg et al. [9] studied CO on HOPG, while Nalezinski et al. investigated monolayers of CF_2Cl_2 [10] and CH_3Cl [11]. We have constructed an apparatus and developed a technique to measure simultaneously IR absorption on one side of a single slab of HOPG and the layer coverage by ellipsometry on the opposite side. In a preliminary survey, we have examined the adsorbates CO, CD_4, C_2D_6, SF_6, and CF_4 from monolayer to bulk coverage. This paper reports results of experiments and calculations of dynamic dipole coupling for CO.

The monolayer phase diagram of CO is known from earlier work, particularly experiments employing LEED [12], X-ray diffraction [13], and heat capacity [14,15]. Marx and Wiechert [16] have given a detailed review. Fig. 1 is a portion of the phase diagram as constructed by Feng and Chan [14]. The high temperature solid phases CD and ID are identified from diffraction experiments [12,13] as triangular lattices with orientational disorder, that is, no long-range orientational order in the plane. These experiments give only limited information on the average molecular orientation with respect to the surface normal. The CD phase is commensurate $(\sqrt{3} \times \sqrt{3})R30°$ with the graphite

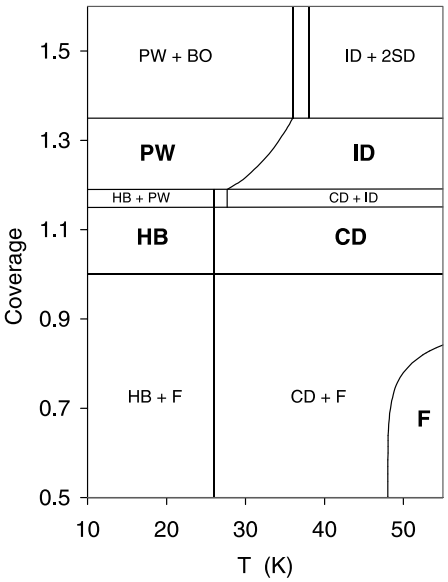

Fig. 1. Partial phase diagram for CO on graphite. Boldface labels indicate single-phase regions: PW = pinwheel, HB = herringbone, ID = incommensurate orientationally disordered, CD = commensurate orientationally disordered, and F = fluid. BO and 2SD are orientationally ordered and disordered bilayer phases.

lattice, while the ID phase is incommensurate, compressed relative to CD.

The HB phase, which occurs below about 26 K at low chemical potential, is commensurate $(2\sqrt{3} \times \sqrt{3})$ and the appearance of only certain superlattice reflections indicates orientational ordering in a "herringbone" pattern, with two molecules per unit cell. The absence of other superlattice reflections that are forbidden by the two glide-plane symmetries of the in-plane herringbone structure implies the absence of long-range-ordered tilt of the molecules out of the plane, with an estimated upper limit of 5° [12]. This does not constrain random or short-range-ordered tilt, either static or dynamic. If static ordered tilt were to occur, it would be the result of spontaneous symmetry breaking driven by the electric quadrupole–quadrupole interaction [17]. Feng and Chan [14] have emphasized the strength of this interaction in CO relative to substrate attraction in accounting for differences from N_2. End-to-end ordering of CO is complete only below about 5 K [18–23], where it should produce corresponding

tilts of a few degrees [24]. Our observation of IR absorption in the HB phase implies that the molecules in fact have a significant r.m.s. out-of-plane component at 20 K, which will be discussed below.

The PW phase, which occurs at low temperatures and higher chemical potential, is believed to have a "pinwheel" structure similar to the (1 1 1) plane of bulk α-CO: One in four molecules is "standing up" with its axis normal to the surface, surrounded by molecules flat on the surface with their axes all angled left (or all right) with respect to the radial direction [12,13]. This structure is incommensurate with the substrate. Both the herringbone and pinwheel structures are consistent with Monte Carlo [25] and energy minimization calculations [24,26] for CO on graphite.

2. Experimental

The cryostat constructed for these studies is similar to our previous ellipsometric cryostat [27a] in that the entire UHV cell surrounding the sample is cooled to within a few degrees of the sample temperature. When adsorbate is introduced into the evacuated cell, adsorption occurs primarily on the sample. To remove the adsorbate, a separate cold finger is cooled below the sample temperature, pulling down the pressure and causing the adsorbate to distill from the sample substrate to the cold finger. This can be accelerated if necessary by briefly heating the sample. To re-adsorb on the sample, the cold finger is simply warmed. By repeating this process, multiple isotherms may be completed without admitting additional gas into the cell. In addition to two windows for ellipsometry, the current UHV cell has a pair of zinc selenide windows for infrared reflection measurements at 70° angle of incidence on the opposite side of the graphite slab. The cell is enclosed in a cryostat vacuum jacket with corresponding sets of windows. A benefit of cooling the entire cell is that outgassing is suppressed and contaminants such as water and CO_2 tend to freeze on the tube leading to the cell before reaching the sample, allowing runs of a month or more duration without warming the sample.

The IR Fourier-transform spectrometer is a Mattson Research Series RS-2 with external focusing optics and detector housed in dry-nitrogen-purged boxes. These components include a rotatable wire grid polarizer (Graseby) and an MCT detector (Graseby). Details of the optical arrangements and techniques are described elsewhere [27b]. To allow access to the cryostat while preserving alignment of the optics, the IR system and the ellipsometer each rest on precision linear bearings and can be moved up to and away from the cryostat. Unless otherwise noted, all spectra were taken with a nominal resolution of 1 cm^{-1}, averaging 100–300 scans requiring a time of 0.7 s per scan.

A $12 \times 12 \times 1$ mm^3 sample of ZXA grade HOPG (Union Carbide) was cleaved with tape and baked ex situ at 700 K for 48 h under flowing argon. After mounting in the cell and evacuation, it was baked in situ overnight at 600 K. Prior to introducing adsorbate gas into the cooled cell, the dynamic background pressure near the pump was $\sim 5 \times 10^{-10}$ Torr and RGA analysis of the background revealed mostly hydrogen. Throughout these runs, sharp layering transitions at chemical potentials comparable to those found in previous work gave a good indication of negligible substrate contamination.

3. Theory

The vibration frequency of a molecule adsorbed on a surface differs from the frequency of a free molecule due to interactions with the substrate and between the adsorbed molecules. The effect of the substrate can be resolved into mechanical and chemical shifts, the former due to impedance of the vibration by the surface and the latter due to changes in the electronic states of the molecule due to coupling to the substrate. In addition there is a dynamic dipole image contribution. Interaction between molecules, in the case of physisorption, is predominantly due to dynamic dipole coupling, which will be analyzed in this section.

First we estimate the order of magnitude of the mechanical and chemical shifts. In a classical mass-and-spring model, the mechanical shift of a

diatomic molecule oriented perpendicular to the surface is approximately

$$\Delta\nu = \nu_{\mathrm{ext}}^2/2\nu_0,$$

where ν_{ext} is the frequency of the normal vibrational mode of the molecule relative to the surface. Using the mode frequencies calculated for nitrogen [28], we estimate the mechanical shift is about $\Delta\nu = +1\ \mathrm{cm}^{-1}$. Tsidoni et al. [29] estimated the chemical shift of a CO molecule oriented perpendicular to the surface as $\Delta\nu = -5.7\ \mathrm{cm}^{-1}$, using the solvation theory of Buckingham [30]. We conclude that there should be a net mechanical plus chemical shift of a few cm^{-1} negative from the free molecule resonance. The "singleton" frequency of an isolated adsorbate molecule on the surface would also include a dynamic dipole self-image contribution, which we estimate from the calculations below as $-1.1\ \mathrm{cm}^{-1}$. As the singleton frequency is not experimentally accessible in this case, we choose to include this contribution with the other dynamic dipole terms calculated below.

The dynamic dipole–dipole interaction between adsorbate molecules produces a frequency shift that can be evaluated by a classical mean field calculation [31,32]. The dipole moment, p, induced in an individual molecule is

$$p = \alpha(E_0 + E_{\mathrm{d}}), \tag{1}$$

where E_0 is the external electric field of the infrared beam and E_{d} is the field at the molecular site due to all of the other molecules:

$$E_{\mathrm{d}}(r_i) = -\sum_{j\neq i} U_{ij}p_j, \tag{2}$$

where $-U_{ij}p_j$ is the field at the site of molecule i due to the dynamic dipole field of molecule j. If all sites are equivalent, $E_{\mathrm{d}} = -Up$ and Eqs. (1) and (2) give

$$p = E_0/(\alpha^{-1} + U). \tag{3}$$

The dipole sum U must be evaluated for each adsorbate structure.

For the case of a single molecular vibration at frequency ν_0 with damping γ, the polarizability has the form

$$\alpha(\nu) = \alpha_{\mathrm{e}} + \frac{\alpha_{\mathrm{V}}}{1 - \left(\frac{\nu}{\nu_0}\right)^2 - \mathrm{i}\gamma\frac{\nu}{\nu_0^2}}, \tag{4}$$

where α_{e} is the electronic polarizability and α_{V} is the vibrational polarizibility.

The normal mode of the monolayer that couples to the external field (i.e., the Brillouin-zone-center mode, in which all of the molecules oscillate in phase) has the frequency ν_1 for which the real part of $(\alpha^{-1} + U)$ is zero. For small damping that is [32]

$$\nu_1 = \nu_0\sqrt{\frac{U\alpha_{\mathrm{V}}}{1 + U\alpha_{\mathrm{e}}} + 1}. \tag{5}$$

Screening of the fields by the substrate is taken into account by including image dipoles in U. As mentioned above, we include also the self-image; this reduces somewhat the sensitivity to the value chosen for d, the distance to the image plane.

The integrated absorbance per molecule of the film is given by

$$A \propto N\nu^2\alpha_{\mathrm{V}}(1 + \alpha_{\mathrm{e}}U)^{-2}, \tag{6}$$

where N is the areal density of adsorbed molecules. The factor involving $\alpha_{\mathrm{e}}U$ represents screening of the field by the electronic polarizability of the other molecules and the images.

In order to get the screening right in the case that the molecular axes are not normal to the surface, we must include explicitly the tensor character of α_{e}. The tensor U is diagonal in an appropriate lattice-based coordinate frame for the high-symmetry lattices of current interest. The polarizability tensor is transformed to this frame and inverted. Then Eq. (3) is replaced by

$$p_z = [\alpha^{-1} + U]^{-1}_{zz}E_0 \equiv \alpha_0(\nu)E_0, \tag{7}$$

where z is the surface-normal direction, and the integrated absorbance is

$$A \propto N\nu^2\alpha_0(\nu).$$

We have evaluated $\alpha_0(\nu)$ numerically for the cases described below.

If the adsorbate lattice has n inequivalent sites, then p becomes an array of n values and U is an n by n matrix, which must be diagonalized to find n zone-center normal modes. For instance, for the

in-plane herringbone structure, the two sites of different azimuth are equivalent through a glide-plane symmetry. However if the molecules on the two sublattices were rotated by *unequal* amounts left and right from a lattice symmetry direction, then the sites would be inequivalent and there would be two modes, whose relative coupling to the external field would depend on the degree of asymmetry. Although we will give no calculations for these cases, some qualitative properties of lattices with inequivalent sites are important. If there are two kinds of sites with different frequencies and they are coupled by positive (negative) off-diagonal terms in U of such magnitude as to produce a frequency shift comparable to the frequency difference, then the peaks repel and oscillator strength is shifted strongly to the higher (lower) frequency mode. If there are many sites with a random distribution of frequencies of width Γ, coupled by positive interactions U_{ij}, then for $U_{ij} \sim \Gamma' = 2\Gamma/v_0\alpha_V$ the absorption spectrum is skewed towards the high-frequency side of the uncoupled spectrum, while for $U_{ij} \gg \Gamma'$ the spectrum is shifted above the uncoupled spectrum and narrowed [33–38].

We have evaluated numerically dipole sums and the resulting frequency shifts for several simple lattice configurations relevant to interpreting the spectra of adsorbed CO monolayers, using Eq. (7). These cases include:

1. The four-sublattice pinwheel structure with molecules on one sublattice perpendicular to the substrate and the other three parallel, so that the latter only contribute through their electronic polarizability.
2. A triangular lattice with equal tilts in random azimuths, approximated by neglecting the horizontal component of the induced field (except the self-image field).
3. A symmetric tilted herringbone, in which all molecules have the same tilt and the tilt azimuth is $+\varphi$ and $-\varphi$ with respect to a symmetry direction for the two sublattices. There are two cases, described in detail in Fig. 4 of You and Fain [12], depending whether the average polarization vector, projected on the surface, is parallel or perpendicular to an adsorbate lattice vector. Following the notation of Kortmann et al. [19], we will designate these DHB II (case a of Ref. [12]) and DHB I (case b) respectively. "DHB" refers to "dipole-oriented herringbone". Kortmann et al. were concerned with C-end-O-end ordering of the CO molecules, with associated small permanent dipole moments, which occurs in an Ising transition at 5.18 K. This is random by 20 K; we are concerned with configurations of induced dipole moments resulting from possible correlated molecular tilts of a different origin.

In these calculations we used the following parameter values: The polarizabilities are the free molecular values [39a], $\alpha_{e\,zz} = 2.33$, $\alpha_{e\,xx} = \alpha_{e\,yy} = 1.80$, $\alpha_V = 0.055$ in units of 10^{-24} cm^3. The intermolecular spacing is $r = 0.426$ nm in the commensurate case and about 0.401 nm for the PW phase [12]. The height of the induced dipole above the image plane is taken to be $d = 0.19$ nm for CO molecules lying (nearly) flat and $d = 0.24$ nm standing up [24,26]. This distance is expected to be slightly larger than half the diameter of the molecule, as the image plane is slightly behind the repulsive "edge" of the surface charge distribution [39b]. Model calculations for herringbone structures [24,26] have shown that azimuthal orientations of approximately $\varphi = \pm 45°$ with respect to a lattice vector give the minimum energy, and we adopt 45°.

We define the tilt angle θ to be the angle between the molecular axis and the surface plane. This convention facilitates the discussion of nearly flat molecules, with which we will be primarily concerned. Fig. 2 shows the calculated absorbances for the two herringbone cases (3) as functions of tilt angle. These absorbances are normalized to the value calculated for the pinwheel, case (1). Fig. 3 shows the corresponding calculated frequency shifts as functions of tilt angle. The dashed lines show the shifts if the horizontal fields of only the six nearest neighbors are included. It turns out that, for the assumed azimuthal orientation of $\varphi = \pm 45°$, case DHB II gives very nearly zero horizontal field projected on the molecular axis at a lattice site. Thus it gives practically the same result as the random case (2) above. The dash-dot

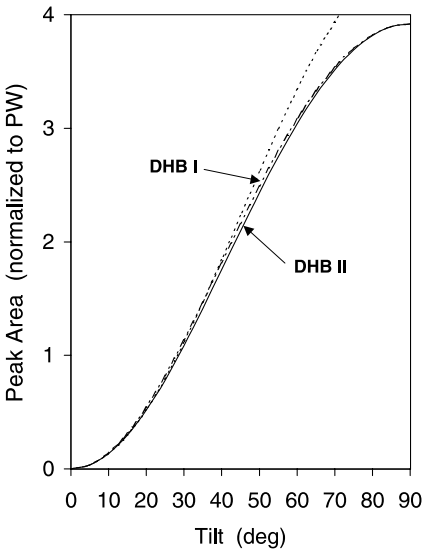

Fig. 2. Calculated integrated absorbance as a function of tilt angle θ from the surface, for two tilt-ordered herringbone monolayer structures. Values are normalized to the calculated absorbance for the PW structure. The short-dashed line is proportional to $\sin^2(\theta)$, fit to the DHB II calculation at small tilt angles θ. The integrated absorbance deviates from this dependence due to the difference in electronic polarizabilities parallel and perpendicular to the molecular axis.

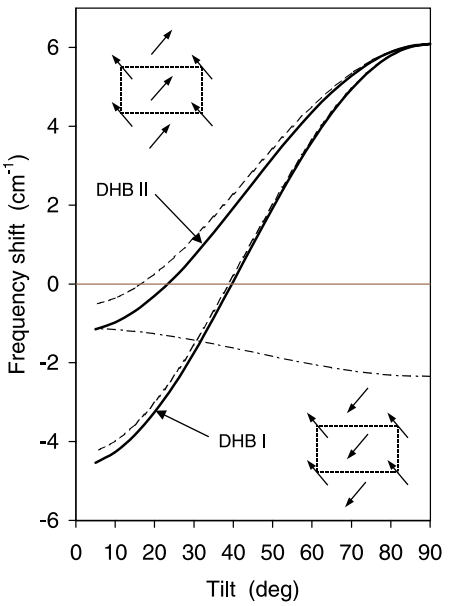

Fig. 3. Calculated frequency shift due to dynamic dipole coupling $\Delta\nu_{DD}$ as a function of tilt angle, for two tilt-ordered herringbone structures, DHB I and DHB II. The molecular orientations are shown in the insets, where the arrow heads indicate the end of the molecule tilted up, and the dotted rectangle is a centered-rectangular unit cell. The dashed curves are calculated omitting horizontal fields due to neighbors beyond the six nearest molecules. The dash-dot curve is the self-image contribution. This calculation uses a fixed image distance, $d = 0.19$ nm.

line is the frequency shift for an isolated molecule due to its self-image. Fig. 3 has been calculated for a fixed image plane distance $d = 0.19$ nm, so is not completely accurate when the θ is not small. The error is largest for $\theta = 90°$, where the self-image contribution is -1.1 cm^{-1} for the correct value $d = 0.24$ nm, nearly equal to the value at $\theta = 0°$ and $d = 0.19$ nm. When this self-image term is combined with the other images there is partial compensation. Insets in Fig. 3 show the two dipole ordering configurations.

It should be noted that the horizontal field interaction is of shorter range than the vertical field interaction. In a (horizontal) planar array, all dipoles pointing vertically upward contribute to the field in the same sense (downward, leading to a positive frequency shift), as do their images so long as they are outside of a cone of 54.7° half-angle. The summed contribution of all dipoles outside radius r falls off asymptotically as $1/r$. For horizontal dipoles, the field of each is nearly canceled by its own image for distances $r \gg 2d$.

4. Experimental results

We recorded ellipsometric coverage isotherms accompanied by a sequence of IRRAS spectra at each of the temperatures 20, 30, 33, 35, 37, and 40 K. Volumetric and ellipsometric isotherm measurements have shown that below 48 K CO forms a maximum of two molecular layers on graphite before the formation of bulk solid [40,41]. Our ellipsometric signal determines unambiguously which spectra correspond to the monolayer, the bilayer, and bulk CO. At 35 K and below, the vapor pressure of CO is less than the 0.1 mTorr resolution of our capacitance manometer. However, by ramping the temperature of the cold finger we can obtain a pressure-ordered sequence of spectra from condensation of the first layer through the second layer to bulk condensation.

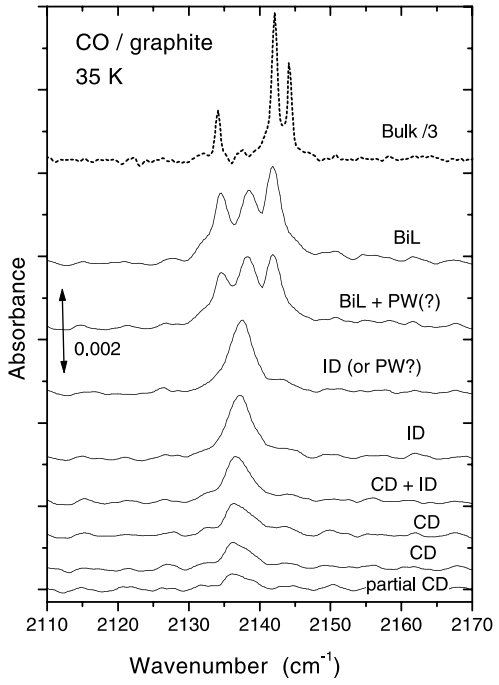

Fig. 4. Sequence of absorption spectra for CO adsorbed on graphite at 35 K. The spectra are offset vertically. Labels on the right are our phase identifications. The nominal resolution is 1 cm^{-1} except for the dashed spectrum which is 0.5 cm^{-1}.

Such a sequence of IR spectra at 35 K is shown in Fig. 4 and is in good agreement with previous work at this temperature by Heidberg et al. [9], who had somewhat better signal-to-noise ratio. At this temperature the saturated vapor pressure of CO is about 10^{-4} Torr and monolayer equilibration through vapor transport is fairly rapid. According to the phase diagram in Fig. 1, the 35 K isotherm should pass through the monolayer CD and ID phases, and a corner of PW just before bilayer condensation. Our lowest spectrum was taken just after the formation of a monolayer and should represent the CD phase. It shows a single absorption peak at 2136.4 cm^{-1} and it is distinctly asymmetric, skewed toward the low-energy side. The significance of this will be discussed later. At a higher pressure the peak position shifts upward to 2137.2 cm^{-1} and its shape becomes more symmetric, while the integrated intensity nearly doubles. We identify this as the ID phase. Shortly before appearance of the bilayer the peak shifts to 2137.6 cm^{-1} and becomes slightly larger, possibly representing the PW phase. Immediately after second layer condensation, as observed by ellipsometry, the single peak splits into three peaks at 2134.6, 2138.2, and 2141.9 cm^{-1}, with total area nearly twice that of the PW peak. At saturation further splitting is observed, with peaks at 2134.1, 2137.2, 2142.1, and 2144.3 cm^{-1} and with increased area.

The 33 K scan should pass through the same sequence of phases and indeed a very similar sequence of spectra was found, including now a distinct PW signature, as seen in Fig. 5. Data at 30 K are not shown here, as the pressure range was more limited, but we obtained a number of spectra characteristic of the ID and then of the PW phase, which are discussed below. Isotherms at 37 and 40 K, Figs. 6 and 7 respectively, show the expected sequence of spectra corresponding to the CD, ID, and bilayer phases. At 40 K a number of vibration–rotation absorption lines of the 3D gas are evident above about 1 mTorr. In the case of the bilayer spectrum the gas contribution has been

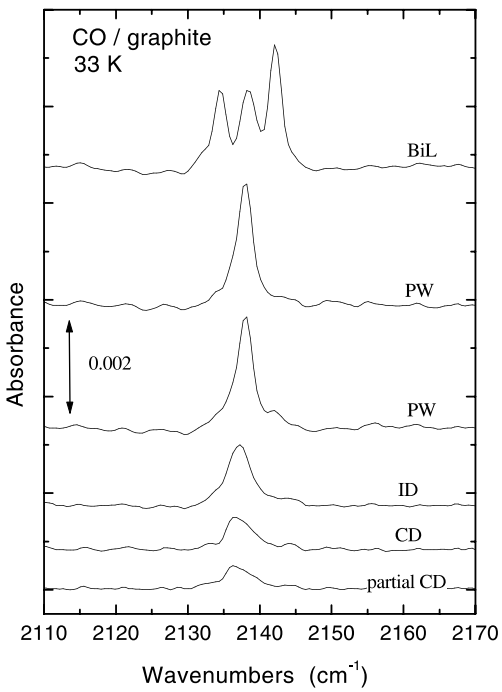

Fig. 5. Sequence of absorption spectra at 33 K.

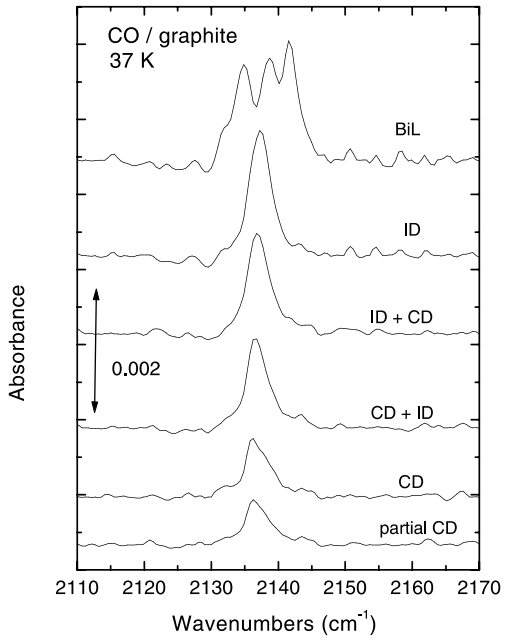

Fig. 6. Sequence of absorption spectra at 37 K.

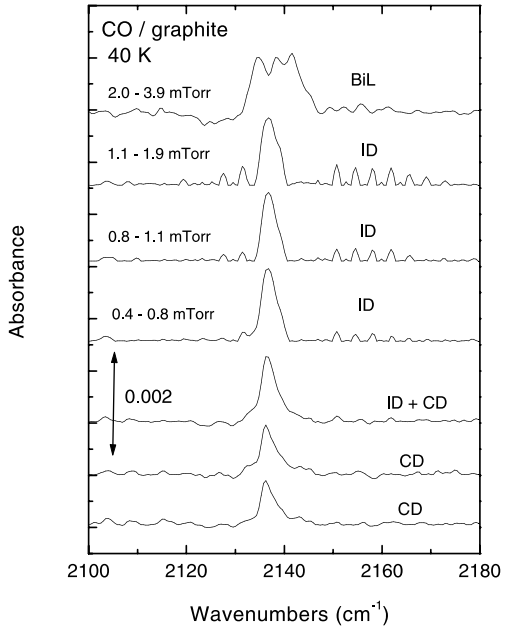

Fig. 7. Sequence of absorption spectra at 40 K. The pressure range during the measurement is indicated on the left.

eliminated by plotting the difference between spectra taken with p- and s-polarization. The 40 K bilayer should be in the "second layer solid orientationally disordered" (2SD) phase, whereas the bilayer below 37 K should be the "bilayer orientationally ordered" (BO) phase. At temperatures much above 40 K, adsorption by the gas in our cell near saturated vapor pressure is sufficiently strong that it becomes difficult to separate gas from the surface absorption even using differences between p- and s-polarization.

Use of the cold finger should provide conditions of imposed pressure (or equivalently, chemical potential), so that first order transitions in the adsorbed film should occur as sharp steps as the cold finger is warmed. However spectra may show coexisting phases if the transition occurs during the averaging time. At very low vapor pressures (below about 10^{-8} Torr) the transport kinetics may create conditions closer to an imposed flux to the sample. This accounts for the transition spectra seen in some of the preceding figures. The latter problem is severe at 20 K, where the saturated vapor pressure is near 10^{-12} Torr.

The 20 K isotherm should pass through the HB and PW phases. Selected spectra are shown in Fig. 8. The initial absorption peak at 2138.2 cm^{-1}

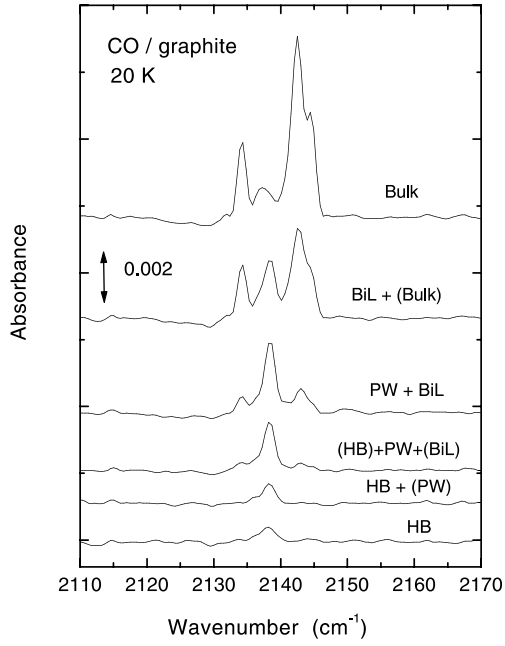

Fig. 8. Sequence of absorption spectra at 20 K.

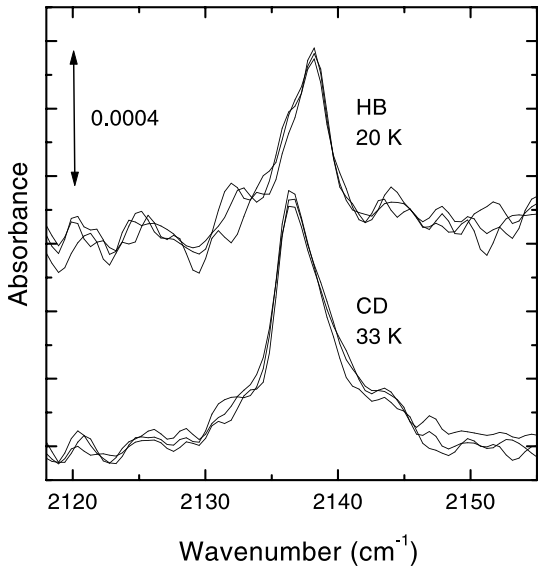

Fig. 9. Three spectra in the HD phase at 20 K and three spectra in the CD phase at 33 K. The baselines here and in the following figure show a small residual contribution from window fringes.

is asymmetric, skewed to the high-energy side. We expect this initial spectrum to be in the HB region. This peak is constant in position and intensity with increasing temperature of the cold finger for a number of spectra, then the position shifts slightly to 2138.5 cm^{-1}, the peak narrows, and the intensity increases substantially. These changes suggest the appearance of the PW phase. Subsequent spectra are characteristic of concurrent growth of PW and bilayer, and of bulk with bilayer. Despite these departures from equilibrium we have obtained, in additional adsorption series, a number of spectra which appear to represent the pure PW and HB phases, several of which are shown in Fig. 9.

5. Interpretation

In each of the monolayer phases there is only a single spectral peak. The parameters of these peaks are summarized in Table 1 by phase and temperature. Frequency shifts Δv are relative to the free-molecule frequency of 2143.10 cm^{-1}. A is the integrated absorbance (peak area). Listed peak

Table 1
Summary of experimental parameters for the surface vibration mode of a CO monolayer

Phase	T (K)	Δv (cm^{-1})	A (cm^{-1})	FWHM (cm^{-1})	Number of spectra
PW	20	−4.63	0.0109	1.0	6
	30	−4.95	0.0104	1.7	7
	33	−5.02	0.0102	2.2	2
HB	20	−4.85	0.0022	3.3	10
CD	33	−6.50	0.0044	4.3	7
	35	−6.70	0.0043	4.1	6
	37	−6.82	0.0041	4.1	5
	40	−6.79	0.0048	3.4	4
ID	30	−5.87	0.0066	3.8	6
	33	−5.93	0.0074	3.6	1
	35	−5.89	0.0083	3.5	1
	37	−5.70	0.0092	3.8	1
	40	−6.39	0.0081	3.8	3

widths (FWHM) are corrected for an instrumental width after apodization of 1.5 cm^{-1}. The fact that absorption is seen at all for the HB, CD, and ID phases implies that the molecules have a significant root-mean-square tilt away from parallel to the surface. In order to quantify this tilt we assume that the nominal structure of the PW phase [12] is correct and use this for calibration.

In the PW phase at 20 K the peak is considerably narrower than in any other monolayer spectrum and appears symmetric within the limitations imposed by background irregularity. This is consistent with the interpretation that there is negligible contribution from the "wheel" molecules and that the "pin" molecules are well ordered. The corresponding dynamic dipole calculation has four sub-lattices, one with molecules standing normal to the surface and the other three with molecules parallel to the surface. The latter contribute only to the electronic screening. At higher temperatures the PW peak broadens substantially, shifts to lower frequency, and decreases somewhat in area. It also becomes slightly skewed to the high-frequency side. The loss in area at 33 K relative to 20 K could be interpreted as a tilt away from the surface normal direction by 15°, to $\theta = 75°$, supplemented by a small contribution from thermal expansion. The broadening might be due to variations in this tilt. Part of the frequency shift can be

attributed to weakening of the dynamic dipole coupling between pin molecules due to both tilt and thermal expansion; however a tilt of $\theta = 75°$ accounts for less than one-fifth of the observed frequency shift and thermal expansion for less. An alternative hypothesis is that the orientational structure is becoming progressively more like that in the ID phase, from which PW is separated by an Ising transition [14]. This would imply a larger tilt of the pin molecules away from the normal, partially compensated by tilt out of the plane of the wheel molecules, leading to more complicated couplings. The contribution of the wheel molecules could account for both the skewness and part of the frequency shift. It is unlikely that ID patches could coexist with PW, unchanged over several spectra, as the film-vapor equilibration time is still only a few seconds at 30 K.

For the nominally flat phases the integrated absorbance depends primarily on the r.m.s. tilt out of the plane and only very slightly on the azimuthal ordering of the tilts (see Fig. 2). In Table 2 we summarize the experimental average peak area A, frequency shift $\Delta\nu_{exp}$, and peak width for each phase. Experimental peak areas, normalized to the peak area for the PW phase at 20 K A_{PW}, are compared to the similarly normalized peak area as a function of tilt angle calculated from the dynamic dipole coupling model, Fig. 2, to obtain the tabulated tilt angles. These tilt angles are then used with the calculated frequency shifts in Fig. 3 to estimate the frequency shift $\Delta\nu_{DD}$ attributable to dynamic dipole coupling in each phase. The result depends on the assumed tilt correlations; we tabulate shifts for DHB I and DHB II tilt ordering. We have not evaluated four-sublattice or larger structures (e.g., DHB III) [19].

For the HB phase the resulting estimate of $\theta = 12°$ for the r.m.s. tilt is more than twice the upper limit estimated by You and Fain [12] for a possible long-range ordered tilt. There are three possible interpretations: The tilts could be uncorrelated; there could be short-range correlations; or there might be long-range ordering plus a random component of comparable magnitude.

The tilt in the CD phase is slightly larger, $\theta = 17°$, and does not change significantly over the temperature range studied. The peak frequency also changes little with temperature, which is consistent with the expectation that the lattice remains commensurate with the substrate. To seek more information as to the nature of the order in the HB and CD phases, we will examine the frequency shifts next. Heat capacity measurements [14] show a broad (FWHM = 2.5 K) rounded peak at the HB–CD transition (in contrast to the analogous transition in N_2, which is sharp). Symmetry arguments [42] predict a first-order transition associated with loss of in-plane herringbone order, which corresponds to singling out one of the six possible ground states (three possible orientations and two-fold sublattice interchange). Monte Carlo calculations [25] show that the quadrupole–quadrupole interaction maintains *local* herringbone-like order well above the transition. This is consistent with X-ray diffraction measurements

Table 2
Determination of molecular tilt from experimental integrated absorbances and comparison of measured frequency shifts with calculated shifts due to dynamic dipole coupling (see text)

Phase	Experimental A (cm^{-1})	$\Delta\nu_{exp}$ (cm^{-1})	FWHM (cm^{-1})	Calculated A/A_{PW}	Tilt, θ (deg)	$\Delta\nu_{DD}$ (cm^{-1})	$\Delta\nu_{exp}$ (cm^{-1}) − 3.6
PW (20 K)	0.0109	−4.63	1.0	(1)	0/90	+0.04	–
HB	0.0022	−4.85	3.3	0.20	12	−4.1 I −0.8 II	−1.25
CD	0.0044	−6.7	4.0	0.40	17	−3.6 I −0.5 II	−3.1
ID	0.0079	−5.9	3.8	0.72	23	−2.8 I +0.1 II	−2.3

$\Delta\nu_{DD}$ is the dynamic dipole shift calculated for both of the herringbone configurations DHB I and DHB II with parameters appropriate for each phase. These values are to be compared to the last column, which is the experimental shift minus a median estimate of the chemical shift.

[13], which found that the superlattice peak indicating that relatively large-scale herringbone order decreases continuously over the range 20 to 40 K. In contrast to the gradual loss of short-range herringbone order, our data on the peak area A indicate that the change in average tilt from the value in the HB phase is essentially complete at 33 K.

Fig. 9 shows three successive HB spectra at 20 K and three successive CD spectra at 33 K, taken under relatively static conditions. The CD peak is nearly 2 cm^{-1} lower in frequency than the HB peak. This is largely due to the fact that the HB peak is skewed to high frequency whereas the CD peak is skewed to low frequency. With the small difference in tilt angle and the same commensurate sites over the graphite substrate, it is unlikely that the chemical shifts are much different for the two phases. The dynamic dipole shift due to the component of local field normal to the surface will shift peaks to higher frequency, and it is larger for the more-tilted CD; i.e., it produces a relative shift is in the wrong direction. This suggests that the in-plane local fields are important. In our calculated frequency shifts (Fig. 3), for tilts of order $\theta = 15°$, tilt ordering of the type DHB II gives a small negative dynamic dipole shift (~ -0.5 cm^{-1}), while ordering of type DHB I gives a substantially larger negative shift (~ -3.5 cm^{-1}). The relevant interaction is short ranged and the difference is little changed if only nearest neighbors are included. Thus if the CD phase had local tilt ordering of type DHB I and the HB phase had local tilt ordering of type DHB II, or random tilts, then a relative shift of the correct sign and right order of magnitude would result. The skewing of the peaks can be interpreted qualitatively by reference to calculations of Persson and Ryberg [32] on substitutionally disordered mixtures of two types of molecules coupled by surface-normal dynamic dipole moments. The varying local environment produces many inequivalent sites and many normal modes which couple in varying degrees with the external field. The positive (in the sense that $U > 0$) mean dynamic dipole coupling causes the oscillator strength to be concentrated towards the high frequency end of the distribution of modes. Model calculations by Tsyganenko et al. [34] show explicitly that skewing is maximized when the mean shift due to dynamic dipole coupling is comparable to the frequency spread due to random interactions. An effect similar to this due to some degree of tilt disorder should account for the skewing of the HB resonance. The CD resonance is skewed in the opposite direction, as would be expected if the mean dynamic dipole coupling were *negative*, which is the case for the dominant local fields in the DHB I-ordered herringbone. This suggests that the CD phase has short-range herringbone order with local DHB I-type correlation of tilts. The HB phase may have short-range (or possibly some long-range) DHB II tilt order, but this is not observable because it produces nearly zero horizontal field coupling.

On account of the low vapor pressure at 20 K, it cannot be ruled out definitively that all of our experimental HB spectra might be actually for HB with coexisting patches of PW. The maximum amount of PW spectrum which can be subtracted without creating a distinct negative spectral region is about 10% of a monolayer. This maximum subtraction would shift the peak down by 1.0 cm^{-1} and make it more symmetric, while reducing the area by 45%. This would reduce the estimated HB tilt to 10°. The preceding conclusions regarding tilt correlations depend largely on the unusual CD spectrum and would not be changed substantially. The CD result, based on multiple spectra at each of four temperatures, is robust.

The ID phase is separated from the PW phase by a second-order Ising-like transition [14] and from CD by a first order transition. The PW phase has long-range order in the choice of sublattice occupied by the upright pin molecules and also the sense of azimuthal rotation of the surrounding wheel molecules. The long-range character of this order must be lost at the transition to the ID phase. Fig. 10 shows three spectra in the PW phase and two in the ID phase, all at 30 K. The ID peak is fairly symmetric, with peak wave number intermediate between those of HB and CD. It has about 80% larger area than the CD peak, indicating larger r.m.s. tilt out of the plane, about 23°. Its more symmetric shape suggests that the ID phase may lack the particular short-range tilt correlations which we postulate for the CD phase.

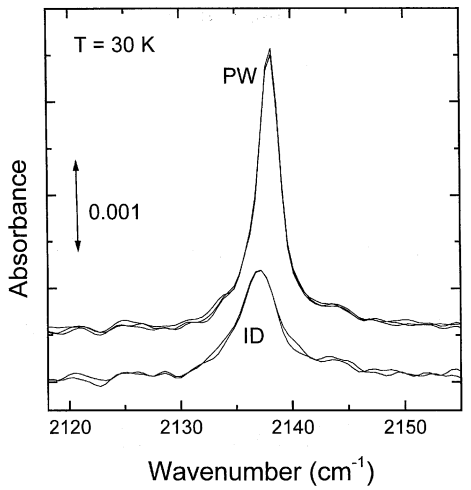

Fig. 10. Three spectra in the PW phase and two spectra in the ID phase at 30 K.

The area of the ID peak increases with temperature, indicating increasing tilt out of the plane. However the peak frequency remains nearly constant (except at 40 K), in contrast to the expectation that it should increase along one of the lines in Fig. 3. Thermal expansion could provide only a small fractional compensation. It is conceivable that tilt correlations that change with temperature could produce a nearly horizontal trajectory in Fig. 3.

The chemical shift can be estimated subtracting the above values for dynamic dipole shift from the experimental frequency shift. For a molecule with axis perpendicular to the surface, consideration of the PW spectra at 20 K gives a chemical shift of -4.7 cm^{-1}) (This includes the mechanical shift but not the self-image shift of about -1.1 cm^{-1}). For molecules with axes (nearly) parallel to the surface, the preceding analysis of the HB and CD spectra is consistent with a chemical shift in the range -4.1 to -3.1 cm^{-1}. A change in chemical shift with tilt an order of magnitude larger than implied by these numbers would be required to cancel the calculated change in dynamic dipole shift in the ID phase.

For the bilayer at three different temperatures below 38 K we find spectra with three well-resolved peaks, similar to that reported by Heidberg and coworkers. Ellipsometry confirms that the appearance of this pattern coincides with condensation of the second layer. Heat capacity measurements [14] place a transition between bilayer phases BO and 2SD at 38 K, but our spectra at 40 and 42 K differ from those at lower temperatures only in that the peaks are slightly broader. The presence of three peaks implies at least three inequivalent sites in the two layers, each with significant r.m.s. tilt, and the absence of strong dynamic dipole coupling between these sublattices. The integrated absorbance implies a mean tilt parameter $\langle \sin^2(\theta) \rangle$ comparable to that in the PW phase. A plausible structure would be a pinwheel-like arrangement in each layer, but with the wheel molecules significantly tilted. This would resemble the bulk α-CO structure. Beyond this we have insufficient information to attempt to model the bilayer structure.

As stated earlier, volumetric [40] and ellipsometric [41] isotherm data show that a third layer is stable relative to bulk α-CO only above 48 K. The four-peak spectrum found at 35 K by Heidberg et al. [9] and in Fig. 4 presumably represents compressed bilayer plus bulk particles, or possibly a trilayer or thicker film of different structure. We have seen hints in ellipsometric scans of additional layering close to saturation but have not studied this systematically. It is possible that a trilayer film reappears somewhere below 38 K with a new structure similar to α-CO. In bulk α-CO spectra measured in transmission, Ewing and Pimentel [43] found a single sharp fundamental peak at 2143.3 cm^{-1}. Jodl et al. [44] reported seeing four lines in the fundamental region for thin macroscopic CO films on a gold surface and they list various mechanisms which might be responsible for the splitting.

6. Conclusions

We have reproduced the sequence of spectra reported by Heidberg et al. [9] for CO films on graphite and shown unambiguously that the three-peak spectrum corresponds to the bilayer. From sequences of spectra at several temperatures between 20 and 40 K, we identify spectra which are

characteristic of each of the four monolayer solid phases known from thermodynamic and diffraction measurements above ~5 K. Combined with calculations of dynamic dipole coupling, these spectra provide estimates of the r.m.s. tilt of the molecules in the three phases in which they nominally lie parallel to the surface.

The fact that the peak for the CD phase is nearly 2 cm^{-1} lower than that for the HB phase, and that this is associated with skewing of the peaks to low and high frequencies respectively, suggests that there must be at least short-range correlations of the tilts that are different in the two phases. Specifically, the CD phase likely has some degree of short-range ordering of type DHB I, while the HB phase has predominantly type DHB II order or no tilt order, either of which would give little horizontal-field coupling between dipoles.

Acknowledgements

Julia Nekrylova assisted in setting up the FTIR system. We have benefited from discussions with A.I. Harrison, V. Celli, and L.W. Bruch and from communications from M.W. Cole and M.J. Bojan. This work was supported in part by National Science Foundation grant DMR9320860 and equipment from the Virginia Higher Education Equipment Trust Fund.

References

[1] J.G. Dash, J. Ruvalds, Phase Transitions in Surface Films, Plenum, New York, 1979.
[2] H. Taub, G. Torzo, H.J. Lauter, S.C. Fain Jr., Phase Transitions in Surface Films 2, Plenum, New York, 1990.
[3] K. Knorr, Phys. Rep. 214 (1992) 113.
[4] Y.J. Chabal, Surf. Sci. Rep. 8 (1988) 211.
[5] A.M. Bradshaw, E. Schweizer, in: R.J.H. Clark, R.E. Hester (Eds.), Spectroscopy of Surfaces, John Wiley and Sons, New York, 1988, p. 413.
[6] R. Ryberg, in: K.P. Lawley (Ed.), Advances in Chemical Physics, John Wiley and Sons, New York, 1989.
[7] J. Heidberg et al., in: E. Umbach, H.J. Freund (Eds.), Adsorption on Ordered Surfaces of Ionic Solids and Thin Films, Springer-Verlag, Berlin, 1993, p. 46.
[8] G.E. Ewing, in: E. Umbach, H.J. Freund (Eds.), Adsorption on Ordered Surfaces of Ionic Solids and Thin Films, Springer-Verlag, Berlin, 1993, p. 57.
[9] J. Heidberg, M. Warskulat, M. Folman, J. Electron. Spectrosc. Relat. Phenom. 54/55 (1990) 961.
[10] R. Nalezinski, A.M. Bradshaw, K. Knorr, Surf. Sci. 331–333 (1995) 255.
[11] R. Nalezinski, A.M. Bradshaw, K. Knorr, Surf. Sci. 393 (1997) 222.
[12] H. You, S.C. Fain Jr., Surf. Sci. 151 (1985) 361.
[13] K. Morishige, C. Mowforth, R.K. Thomas, Surf. Sci. 151 (1985) 289.
[14] Y.P. Feng, M.H.W. Chan, Phys. Rev. Lett. 71 (1993) 3822.
[15] A. Inaba, T. Shirakami, H. Chihara, J. Chem. Thermodyn. 23 (1991) 461.
[16] D. Marx, H. Wiechert, in: I. Prigogine, S.A. Rice (Eds.), Surface Properties, Advances in Chemical Physics, vol. 95, Wiley, New York, 1996, p. 213.
[17] A.B. Harris, A.J. Berlinsky, Can. J. Phys. 57 (1979) 1852.
[18] A. Inaba, T. Shirakami, H. Chihara, Chem. Phys. Lett. 146 (1988) 63.
[19] K.D. Kortmann, B. Leinbock, H. Wiechert, S.C. Fain, N. Stusser, Physica B 234–236 (1997) 167.
[20] H. Wiechert, S.-A. Arlt, Phys. Rev. Lett. 71 (1993) 2090.
[21] H. Wiechert, K.D. Kortmann, Surf. Sci. 441 (1999) 65.
[22] D. Marx, S. Sengupta, P. Nielaba, K. Binder, Phys. Rev. Lett. 72 (1994) 262.
[23] D. Marx, S. Sengupta, P. Nielaba, K. Binder, Surf. Sci. 321 (1994) 195.
[24] J. Belak, K. Kobashi, R.D. Etters, Surf. Sci. 161 (1985) 390.
[25] C. Peters, M.L. Klein, Mol. Phys. 54 (1985) 895.
[26] F.Y. Hansen, L.W. Bruch, S.E. Roosevelt, Phys. Rev. B 45 (1992) 11238.
[27] (a) H.S. Youn, X.F. Meng, G.B. Hess, Phys. Rev. B 48 (1993) 14556;
(b) D.A. Boyd, Ph.D. thesis, University of Virginia, 1998, unpublished.
[28] T.H.M. van den Berg, A. van der Avoird, Phys. Rev. B 43 (1991) 13926.
[29] E. Tsidoni, Y. Kozirovski, M. Folman, J. Heidberg, J. Electron. Spectrosc. Relat. Phenom. 44 (1987) 89.
[30] A.D. Buckingham, Trans. Faraday Soc. 56 (1960) 753.
[31] G.D. Mahan, A.A. Lucas, J. Chem. Phys. 68 (1978) 1344.
[32] B.N.J. Persson, R. Ryberg, Phys. Rev. B 24 (1981) 6954.
[33] V.A. Ermoshin, A.K. Kazanskii, Opt. Spectrosc. 75 (1993) 719.
[34] Y.A. Tsyganenko, V.A. Ermoshin, M.R. Keyser, K.S. Smirnov, A.A. Tsyganenko, Vib. Spectrosc. 13 (1996) 11.
[35] B.N.J. Persson, J. Electron. Spectrosc. Relat. Phenom. 54–55 (1990) 81.
[36] B.N.J. Persson, F.M. Hoffmann, J. Electron. Spectrosc. Relat. Phenom. 45 (1987) 215.
[37] P. Jakob, J. Chem. Phys. 108 (1998) 5035.
[38] P. Jakob, B.N.J. Persson, Phys. Rev. Lett. 78 (1997) 3503.
[39] (a) C.G. Gray, K.E. Gubbins, Theory of Molecular Fluids, Clarendon, Oxford, 1984;
(b) N.D. Lang, W. Kohn, Phys. Rev. B 7 (1973) 3541.

[40] Y. Larher, F. Angerand, Y. Maurice, J. Chem. Soc., Faraday Trans. I 83 (1987) 3355.
[41] H. Wu, Ph.D. thesis, University of Virginia,1995, unpublished.
[42] M. Schick, Surf. Sci. 125 (1983) 94.
[43] G.E. Ewing, G.C. Pimental, J. Chem. Phys. 35 (1961) 925.
[44] H.J. Jodl, W. Loewen, D. Griffith, Solid State Commun. 61 (1987) 503.